Molecular Therapy
Methods & Clinical Development
Original Article

Efficacy, pharmacokinetics, and safety in the mouse and primate retina of dual AAV vectors for Usher syndrome type 1B

Rita Ferla,[1,2,11,12] Fabio Dell'Aquila,[1,12] Monica Doria,[1] Maria Ferraiuolo,[3] Alessia Noto,[3] Fabiana Grazioli,[3] Virginia Ammendola,[3] Francesco Testa,[4] Paolo Melillo,[4] Carolina Iodice,[1] Giulia Risca,[5] Novella Tedesco,[6,7] Pierre Romain le Brun,[6,7] Enrico Maria Surace,[8] Francesca Simonelli,[4] Stefania Galimberti,[5] Maria Grazia Valsecchi,[5] Jean-Brice Marteau,[9] Philippe Veron,[6,7] Stefano Colloca,[3] and Alberto Auricchio[1,2,10,11]

[1]Telethon Institute of Genetics and Medicine (TIGEM), Via Campi Flegrei 34, 80078 Pozzuoli, Italy; [2]AAVantgarde BIO Srl, 20123 Milan, Italy; [3]ReiThera Srl, 00128 Rome, Italy; [4]Eye Clinic, Multidisciplinary Department of Medical Surgical and Dental Sciences, University of Campania "Luigi Vanvitelli", 80131 Naples, Italy; [5]Center of Biostatistics for Clinical Epidemiology, School of Medicine and Surgery, University of Milano-Bicocca, 20900 Monza, Italy; [6]Genethon, 91000 Evry, France; [7]Université Paris-Saclay, University Evry 91000, INSERM, Genethon, Integrare Research Unit UMR_S951, 91000 Evry, France; [8]Medical Genetics, Department of Translational Medicine, University of Naples "Federico II", 80131 Naples, Italy; [9]Genosafe, 91000 Evry, France; [10]Department of Advanced Biomedical Sciences, "Federico II" University, 80131 Naples, Italy

Gene therapy of Usher syndrome type 1B (USH1B) due to mutations in the large *Myosin VIIA* (*MYO7A*) gene is limited by the packaging capacity of adeno-associated viral (AAV) vectors. To overcome this, we have previously developed dual AAV8 vectors which encode human *MYO7A* (dual AAV8.*MYO7A*). Here we show that subretinal administration of 1.37E+9 to 1.37E+10 genome copies of a good-manufacturing-practice-like lot of dual AAV8.*MYO7A* improves the retinal defects of a mouse model of USH1B. The same lot was used in non-human primates at doses 1.6× and 4.3× the highest dose proposed for the clinical trial which was based on mouse efficacy data. Long-lasting alterations in retinal function and morphology were observed following subretinal administration of dual AAV8.*MYO7A* at the high dose. These findings were modest and improved over time in the low-dose group, as also observed in other studies involving the use of AAV8 in non-human primates and humans. Biodistribution and shedding studies confirmed the presence of vector DNA mainly in the visual pathway. Accordingly, we detected human MYO7A mRNA expression predominantly in the retina. Overall, these studies pave the way for the clinical translation of subretinal administration of dual AAV vectors in USH1B subjects.

INTRODUCTION

Retinal gene therapy with adeno-associated viral (AAV) vectors has emerged as safe and effective in humans, with one approved product[1] and several more in advanced phases of clinical development for a number of inherited retinal diseases (IRDs) including: achromatopsia,[2] choroideremia,[3] Leber hereditary optic neuropathy,[4] age-related macular degeneration,[5] X-linked retinitis pigmentosa,[6] and X-linked retinoschisis,[7] among others. However, as the DNA cargo capacity of AAV vectors is 4.7 kb,[8] IRDs caused by mutations in genes with coding sequences (CDS) that exceed this capacity cannot be treated with a single AAV vector. We have previously shown that subretinal delivery of dual hybrid AAV vectors, each carrying one-half of a large expression cassette up to 9 kb in size, efficiently transduce the retina of small and large animal models.[9,10] This occurs as a result of AAV DNA tail-to-head concatemerization mediated by both AAV inverted terminal repeats (ITRs) and/or recombination through highly recombinogenic sequences followed by their splicing from the reconstituted mature mRNA.[9,10]

We developed dual hybrid AAV8 vectors (hereafter named dual AAVs) to treat retinitis pigmentosa (RP) associated with Usher syndrome type 1B (USH1B; MIM:#276900). USH1B is caused by biallelic mutations in the *MYO7A* gene which encodes the large unconventional Myosin VIIA (MYO7A) motor protein.[11–13] USH1B patients are born with congenital hearing impairment or are completely deaf and have prepubertal onset of RP.[14] While cochlear implants are available to counteract deafness, no treatment is currently available for RP.

We have previously shown that subretinal administration of dual AAV serotype 8 (AAV8) encoding for *MYO7A* (dual AAV8.*MYO7A*)

Received 9 November 2022; accepted 7 February 2023;
https://doi.org/10.1016/j.omtm.2023.02.002.

[11]Senior author

[12]These authors contributed equally

Correspondence: Rita Ferla, Telethon institute of Genetics and Medicine (TIGEM), Via Campi Flegrei 34, 80078 Pozzuoli, Italy; AAVantgarde BIO Srl, 20123 Milan, Italy
E-mail: rita.ferla@aavantgardebio.com
Correspondence: Alberto Auricchio, Telethon institute of Genetics and Medicine (TIGEM), Via Campi Flegrei 34, 80078 Pozzuoli, Italy; AAVantgarde BIO Srl, 20123 Milan, Italy.
E-mail: auricchio@tigem.it

results in the reconstitution and expression of full-length human MYO7A in both mice and pigs[9,10] and improves the retinal defects of the shaker1 (sh1) mouse model of USH1B.[9]

Our aim is to translate retinal gene therapy with dual AAV8.*MYO7A* into patients with USH1B RP. In view of this, we performed a dose-response study in sh1 mice to select three doses of dual AAV8.*MYO7A* to be translated to USH1B subjects taking into account that the human retinal surface is around 100-fold larger than that of mice.[15,16] In view of a first-in-human trial of dual AAV vectors, we have performed safety, biodistribution, and expression studies in non-human primates (NHPs) which have a similar eye size and retinal structure as humans, including the presence of the macular region shared only among primates. Here, we demonstrate that subretinal administration of a good manufacturing practice (GMP)-like lot of dual AAV8.*MYO7A* improves USH1B retinal defects in mice and has a safety, biodistribution, and expression profile in NHPs that supports its use in humans.

RESULTS

Production and preclinical testing of GMP-like dual AAV8.*MYO7A*

We performed non-clinical studies using a lot of dual AAV serotype 8 vector encoding the human *Myosin VIIA* (dual AAV8.*MYO7A*) produced according to a process that is similar to the GMP process employed for the clinical lot (hereafter referred to as GMP-like lot). The lot was produced by triple transfection of adherent human embryonic kidney 293 cells expressing the SV40 large T antigen (HEK293T) followed by two rounds of cesium chloride ultracentrifugation. AAV8 vectors encoding the 5′ half and the 3′ half of *MYO7A* (AAV8.5′*MYO7A* and AAV8.3′*MYO7A*) were produced separately, dialyzed, and formulated in the final formulation buffer, i.e., PBS supplemented with 35 mM NaCl and 0.001% P188. AAV8.5′*MYO7A* and AAV8.3′*MYO7A* vectors were then quantified by qPCR, mixed in a 1:1 ratio, and 0.22-μm filtered to generate the dual AAV8.*MYO7A* GMP-like lot. Table S1 reports the characteristics of this lot.

The efficacy of the GMP-like lot of dual AAV8.*MYO7A* was assessed by subretinal administration to shaker1 (sh1) mice to select the doses to be translated in USH1B patients. Its safety, immunogenicity, biodistribution, and expression were assessed in NHPs.

Dual AAV8.*MYO7A* dose response in shaker1 mice

To select the dual AAV8.*MYO7A* vector doses to be tested in a future phase I/II clinical trial in USH1B subjects, we performed an efficacy dose-response study in sh1$^{-/-}$ mice. sh1$^{-/-}$ eyes received one of the following dual AAV doses: 1.37E+9, 4.4E+9, or 1.37E+10 total genome copies (GC)/eye. A scheme of dual AAV8.*MYO7A* vectors is reported in Figure 1A. Unaffected heterozygous (sh1$^{+/-}$) and affected (sh1$^{-/-}$) mice injected with the AAV vehicle were used as positive and negative controls, respectively. sh1$^{-/-}$ mice display ultrastructural defects of the retina, as almost no melanosomes are located to the retinal pigment epithelium (RPE) apical villi.[9,17] Three months post-injection, we measured the number of correctly localized melanosomes to the RPE apical villi (Figure 1B). Subretinal injection of the two highest doses of dual AAV8.*MYO7A* significantly improved retinal defects compared with sh1$^{-/-}$ that received the AAV vehicle with affected eyes treated with the highest dose (Figure 1C) showing no statistical difference from unaffected eyes. Sh1$^{-/-}$ treated with the lowest dose also showed correction of melanosome localization compared with the negative control, although this difference was not statistically significant. This was due to variability within the unaffected sh1$^{+/-}$ group; indeed when we excluded from the analysis unaffected sh1$^{+/-}$, eyes treated with the lowest dose also had a significantly ($p < 0.01$) higher number of properly localized melanosomes compared with negative controls. Western blot analysis of lysed eyecups (RPE + neural retina) from sh1$^{-/-}$ mice 5 weeks after subretinal injection displays expression of full-length MYO7A protein at all selected doses of dual AAV8.*MYO7A* (Figure 1D). A higher number of eyes had detectable MYO7A expression at 1.37E+10 and 4.4E+9 GC/eye than at 1.37E+9 GC/eye (Figure 1E). The highest dose tested induced significantly ($p < 0.01$) higher levels of MYO7A expression compared with the other doses (Figure 1E). In addition, quantification of the intensity of the MYO7A protein bands showed that subretinal administration of dual AAV at the low/intermediate and high doses resulted in about 40% and 67% of the levels of endogenous mouse Myo7A protein detected in sh1$^{+/-}$ eyes, respectively (Figure 1E). Based on these results and on the assumption that the mouse retinal area is about 100-fold smaller than that of humans, we are considering the following three doses of dual AAV8.*MYO7A* for use in humans: 1.37E+11, 4.44E+11, and 1.37E+12 total GC/eye.

Dual AAV8.*MYO7A* biodistribution, shedding, and expression following subretinal administration in NHPs

The pharmacokinetics (biodistribution, including shedding and germline transmission analysis, and expression) of the GMP-like lot of dual AAV8.*MYO7A* was evaluated in a good laboratory practice (GLP)-compliant study following subretinal administration in cynomolgus macaques (Table 1). Animals were administered with either a low dose (LD, 1.37E+12 total GC/eye) or high dose (HD, 3.75E+12 total GC/eye) of dual AAV8.*MYO7A* or with the AAV vehicle (CTR) in their right eyes. Left eyes were left untreated as controls (Table 1). Based on the difference in retinal area between macaques and humans,[18,19] the LD and HD in NHPs correspond to 1.6× and 4.3× the HD proposed for a future clinical trial.

Since the target organ of dual AAV8.*MYO7A* is the eye and AAV vectors are not expected to spread to non-ocular tissues following subretinal injection,[20–23] biodistribution was focused on ocular tissues and components of the visual pathway and on a selected subset of non-ocular tissues, and in tears and serum (to assess vector shedding). Tissues in the LD group that tested positive to both AAV vectors (i.e., AAV8.5′*MYO7A* and AAV8.3′*MYO7A*) were also analyzed for expression of the reconstituted human MYO7A mRNA.

As expected, both AAV8.5′*MYO7A* and AAV8.3′*MYO7A* DNA were mainly found in the retina of eyes receiving either the LD or the HD, and in particular in the bleb area, where the difference in

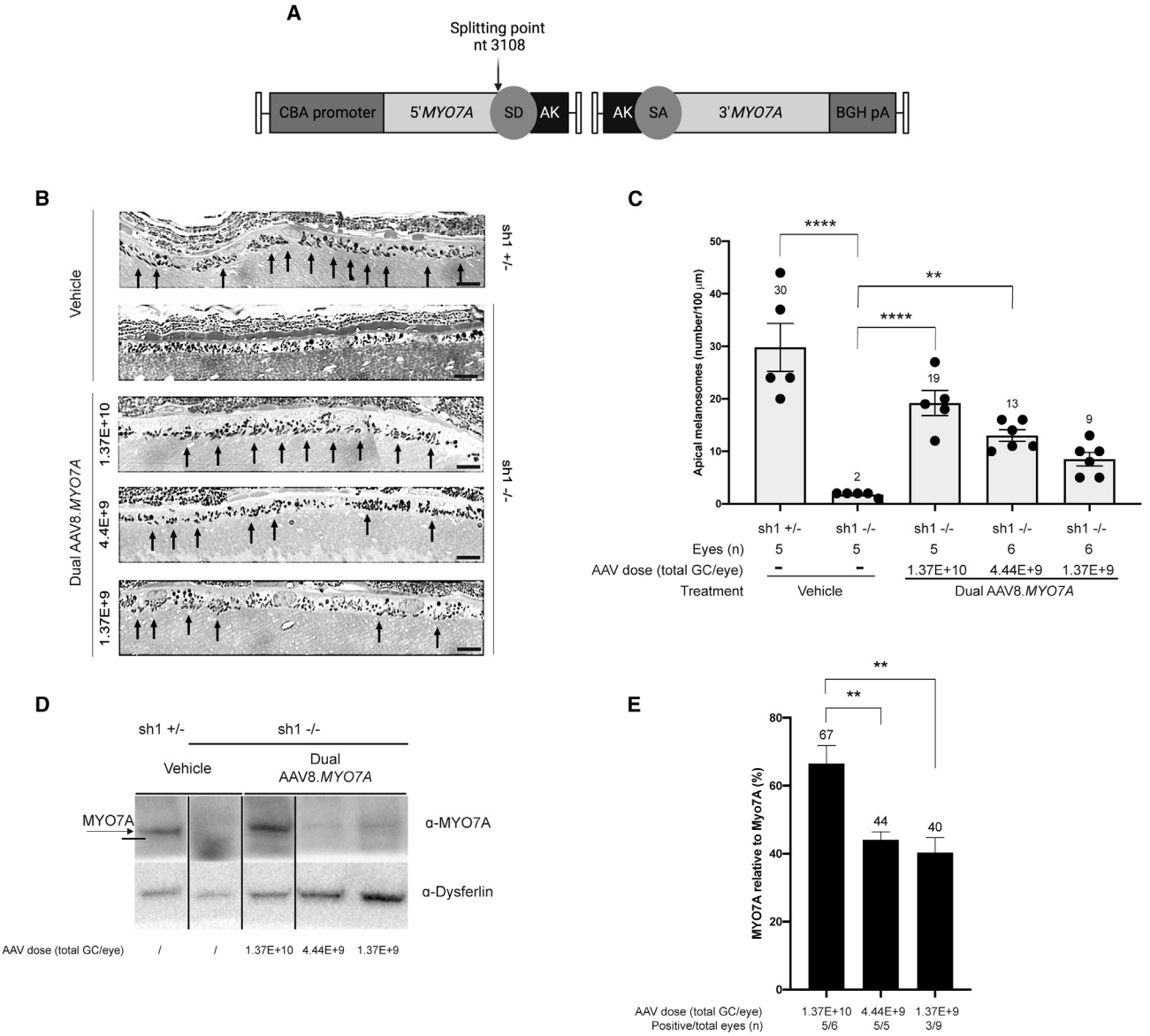

Figure 1. Dose-dependent improvement of apical melanosome localization and increase of MYO7A protein expression in shaker1 mice

(A) Scheme depicting the AAV8.5′*MYO7A* and AAV8.3′*MYO7A* vectors. Black arrow indicates MYO7A splitting point (cartoon drawn using BioRender.com). nt, nucleotide; CBA, chicken β-actin promoter; MYO7A, human MYO7A coding sequence; SD, splicing donor signal; SA, splicing acceptor signal; AK, F1 phage recombinogenic region; BGH pA, bovine growth hormone polyadenylation signal. (B) Semi-thin retinal sections stained with toluidine blue representative of sh1$^{+/-}$ receiving a subretinal injection of vehicle, as positive control, or of sh1$^{-/-}$ receiving a subretinal injection of either vehicle, as negative control, or dual AAV8.*MYO7A* at either 1.37E+10, 4.4E+9, or 1.37E+9 total genome copies (GC)/eye. Black arrows point at correctly localized melanosomes. The scale bars represent 10 μm. (C) Quantification of melanosome localization in the RPE villi of whole retina sections of sh1 mice 3 months after treatment. The number of apical melanosomes/100 μm of RPE is reported. Data are presented as single measurement for each eye (dot) and as mean ± SEM (column). Statistical analyses were conducted using one-way ANOVA followed by the Tukey post hoc test. p value versus sh1$^{-/-}$ receiving the solvent is **p < 0.01, ****p < 0.0001. (D) Representative western blot analysis of sh1$^{-/-}$ eyecups 5 weeks after subretinal delivery of dual AAV8.*MYO7A* at the doses of 1.37E+10, 4.4E+9, or 1.37E+9 total GC/eye. As positive and negative controls, sh1$^{+/-}$ and sh1$^{-/-}$ received a subretinal injection of vehicle (same volume as dual AAV), respectively. α-MYO7A, western blot with anti-Myosin VIIA antibody; α-dysferlin, western blot with anti-dysferlin antibody, used as loading control. (E) Quantification of MYO7A levels expressed in sh1$^{-/-}$ eyecups 5 weeks following subretinal injection of dual AAV8 vectors as percentage (%) of endogenous Myo7a expressed in littermate sh1$^{+/-}$ eyes receiving a subretinal injection of vehicle. Data are presented as mean ± SEM. All eyes (n = 12) used for the quantification are positive for Myo7A expression, and no negative control eyes (n = 6) have detectable expression of Myo7A. The quantification was performed by western blot analysis using the anti-MYO7A antibody and measurements of MYO7A and Myo7a band intensities normalized to dysferlin. p value of 1.37E+10 versus 4.4E+9 or 1.37E+9 is **p < 0.01.

Table 1. NHPs experimental groups and treatment

Group	Dose (total GC/eye)	Treatment		No. of animals
		Left eye	Right eye	
CTR	–	untreated	AAV vehicle	4M + 4F
LD	1.37E+12	untreated	dual AAV8.*MYO7A*	6M + 6F
HD	3.75E+12	untreated	dual AAV8.*MYO7A*	4M + 4F

GC, genome copies; CTR, AAV vehicle group; LD, low-dose group; HD, high-dose group; M, male; F, female.

terms of GC between the two groups mirrors the difference in terms of doses administered (about 3-fold) (Figures 2A and 2B). Dual AAV8.*MYO7A* GC were on average 1 log lower in the non-bleb than in the bleb retina area, although animals in the LD group showed a higher variability in terms of GC in the non-bleb compared with the bleb area (Figures 2A and 2B). In animals receiving the LD, dual AAV DNA was found in the (right) anterior segment, optic nerve, vitreous fluid, and, more variably, in the optic muscle but at levels 3–4 logs lower than those measured in the injected retina area (Figures 2A and 2B). Dual AAVs were detected in the optic tracts (both left and right), lenses (both right and left), lateral geniculate nucleus (both left and right), optic chiasm, and right thalamus at levels either close to or below the limit of quantification (LOQ) (Figures 2A and 2B). More spreading outside the retina was found in the HD compared with the LD group as dual AAV DNA was found in the right anterior segment, vitreous fluid, and optic muscle and in the right lens and optic nerve at levels 1 and 2–3 logs lower, respectively, than those observed in the bleb area (Figures 2A and 2B). In general, the spreading outside the retina toward ocular tissues and components of the ocular pathways was similar in terms of tissues involved between the LD and HD groups (except for superior colliculus and right thalamus, where vectors were detected only in the HD or the LD group, respectively), while the GC measured in these tissues were dose-dependent (Figures 2A and 2B). Dual AAV DNA was undetectable in the retina, anterior segment, optic nerve, and optic muscle of the left untreated eye, in the left thalamus, and in the occipital cortex and cerebellum of both LD and HD groups (Tables S2–S9). Importantly, vectors spreading through the ocular pathway were overall negligible. Figure 2C shows a cartoon of the visual pathway summarizing dual AAV biodistribution.

Spreading of dual AAVs outside the visual system was minimal and occurred potentially through the lymphatic system as suggested by dual AAV DNA presence in the parotid, mandibular lymph nodes, spleen, and mesenteric lymph nodes, although at levels lower (3–5 logs) than in the retina (Figures 2A and 2B). AAV8.3′*MYO7A* DNA was detectable in the liver of the macaques of the HD group at various levels, and in one macaque in the LD group at levels below LOQ (Figures 2A and 2B). No vector was detected in blood, pancreas, jejunum, muscle, heart, lung, and kidneys as well as ovary, testis, and epididymis, indicating a negligible risk of germline transmission (Tables S6–S9). Dual AAV DNA was below the limit of detection (LOD) in tissues from animals in the CTR group (data not shown).

Expression of dual AAV8.*MYO7A* was mainly restricted to the retina (bleb and non-bleb areas) (Figure 2D). Human MYO7A mRNA was also measured in the right optic nerve but at levels 4 logs lower than those found in the retina (Figure 2D). Highly variable levels of expression (from 4 to 6 logs lower or <LOQ) were found in optic muscle and anterior segment right, optic tracts, and chiasm while no expression was found in other ocular and non-ocular tissues that were positive for dual AAV DNA (Figure 2D).

Shedding in tears of right eyes administered with dual AAV8.*MYO7A* was dose-dependent in terms of both GC and persistence (Figures 3A and 3B). Dual AAV DNA was detectable (at levels close or below the LOQ) in tears from eyes receiving either LD or HD up to 31 and 61 days post injection, respectively, although in tears from one HD-treated eye very low but still detectable levels were found up to 91 days post-injection (Figures 3A and 3B). Dual AAV DNA was also measured in tears from untreated left eyes but at levels 1–2 logs lower than those observed in the treated right eyes and with faster clearance in the LD group (Figures 3A and 3B). These findings indicated that vector shedding may easily occur from treated to untreated eyes likely by eye rubbing. Finally, low levels of dual AAV DNA were also found in tears from right eyes receiving the vehicle control (Figure 3C). This finding can be attributed to viral shedding from dual AAV8.*MYO7A*-treated control macaques considering that they were housed in the same room. Other tissues and fluids from animals administered with the AAV vehicle (CTR group) were free of vector, excluding an error of dosing (data not shown).

Dual AAV DNA was also detected in serum of both LD- and HD-treated animals up to 15 days post injection and became undetectable from 31 days post injection (Figure S1); no clear differences in terms of both persistence and amount of DNA was observed between the LD and HD groups. No dual AAV DNA was found in serum from the CTR group (data not shown).

Ocular and systemic findings following subretinal administration of dual AAV8.*MYO7A* in NHPs

Ophthalmoscopic analysis of eyes administered with either dual AAV8.*MYO7A* or AAV vehicle showed intraocular inflammatory responses characterized by aqueous flare, aqueous cells, vitreous cells, and vitreous haze (Tables S10–S12). These initial acute procedure-related responses were generally comparable across all experimental groups up to days 10–12, after which a greater anterior and posterior segment inflammatory response was documented in eyes administered with dual AAV8.*MYO7A* compared with eyes administered with the AAV vehicle (Tables S10–S12). Findings in eyes from the LD group were comparable with those from the HD group. However, some findings showed higher incidence in HD- than in LD-treated eyes. Indeed, perivascular sheathing was observed in 4 out of 8 (50%) and in 2 out of 12 (17%) eyes receiving the HD and the LD, respectively (Tables S11 and S12). Similarly, RPE pigment alteration

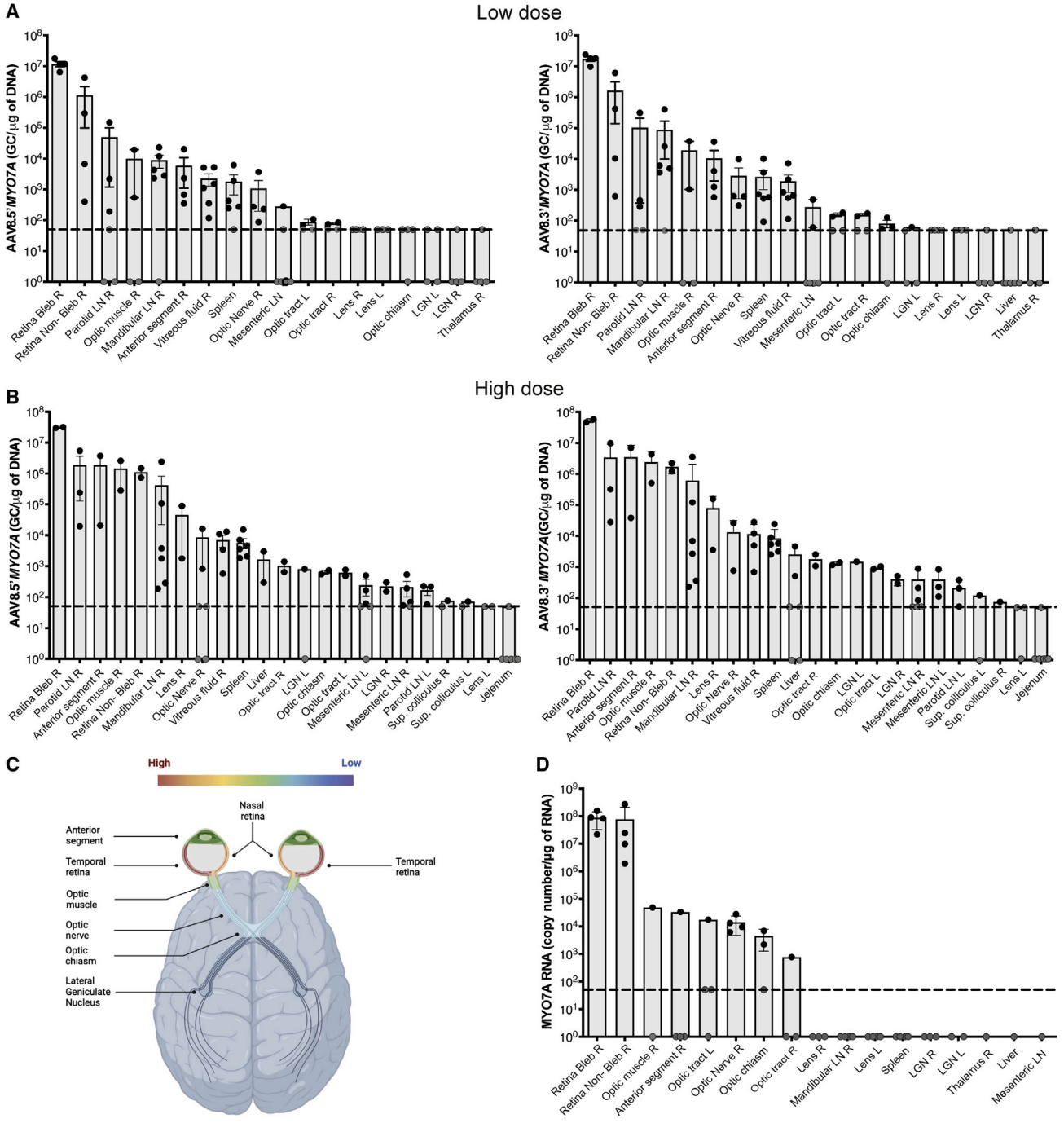

Figure 2. Dual AAV8.*MYO7A* biodistribution and expression following subretinal administration in NHPs

(A and B) Dual AAV8.*MYO7A* biodistribution was evaluated in a panel of ocular and non-ocular tissues from male and female NHPs administered with the low dose (LD) (A) or high dose (HD) (B). qPCR was performed on both AAV8.5′*MYO7A* DNA (left panel) and AAV8.3′*MYO7A* (right panel). Data are presented as single measurements for each sample (circle) and as mean ± SEM (column) for values above the limit of quantification, >LOQ, and in a decreasing order of dual AAV levels. The LOQ and LOD are 50 and 15 GC/μg total DNA, respectively. Samples above LOQ are represented as black circles, and samples below LOQ are represented as gray circles. The area under the LOQ is highlighted by the dotted line. Only tissues with dual AAV DNA levels at least >LOQ were reported in the graph; tissues where dual AAV DNA was <LOD are shown in Tables S2–S9. R, right; LN, lymph node; L, left; LGN, lateral geniculate nucleus; Sup, superior. (C) Cartoon of the visual pathway showing AAV biodistribution from high (red) to low (blue) genome copy levels (cartoon drawn using BioRender.com). (D) *MYO7A* expression was evaluated by qRT-PCR of MYO7A mRNA in tissues from the LD group that were positive for both AAV.5′*MYO7A* DNA and AAV.3′*MYO7A* DNA. Data are presented as single measurements for each sample (circle) and as mean ± SEM (column)

(legend continued on next page)

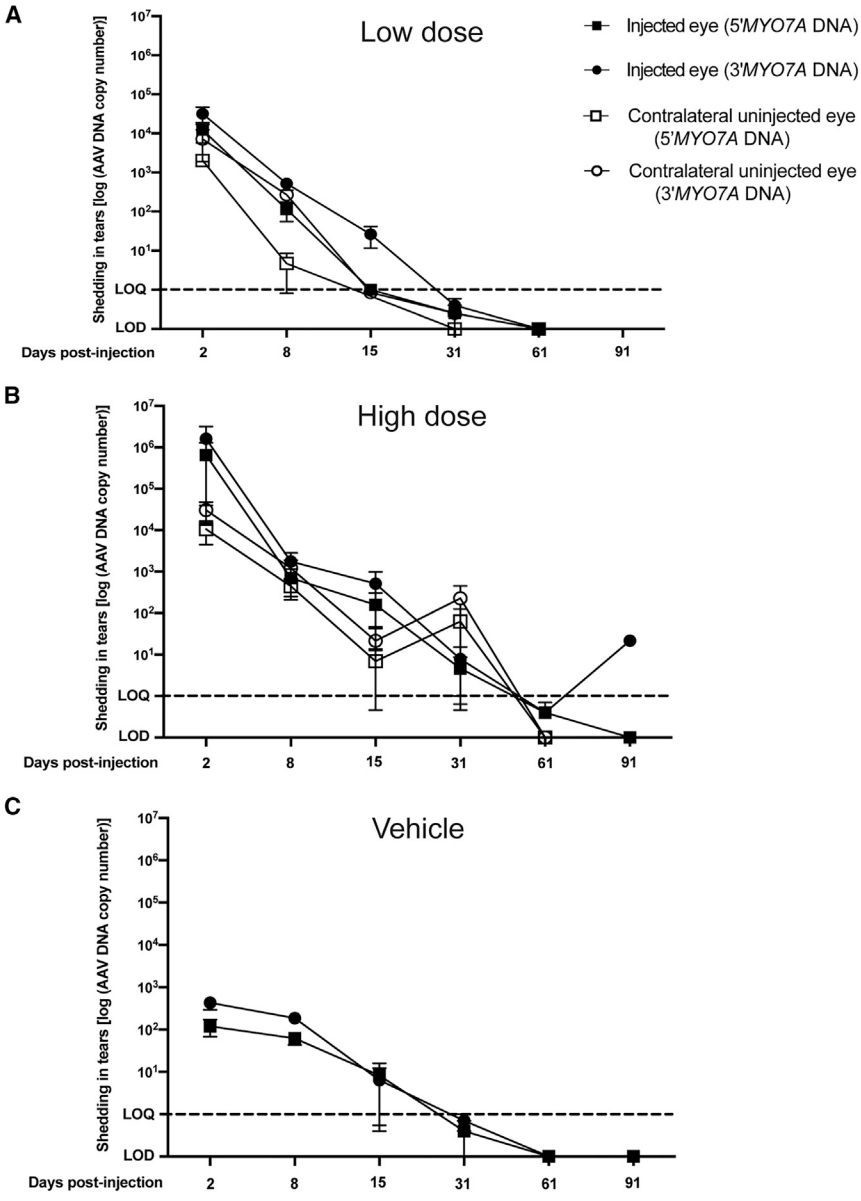

Figure 3. Dual AAV8.*MYO7A* shedding in tears of NHPs following subretinal administration

Dual AAV8.*MYO7A* shedding was analyzed on tears of animals from the LD (A), the HD (B), or the vehicle (CTR) (C) groups by qPCR at 2, 8, 15, 31, 61, and 91 days post injection. Tears from contralateral uninjected eyes of animals receiving the AAV vehicle were not collected. Data are presented as mean ± SEM; mean values are shown as squares for AAV8.5′*MYO7A* DNA and as circles for AAV8.3′*MYO7A* DNA. The LOQ is 20 AAV GC/well and the LOD is 6 AAV GC/well. The area under the LOQ is highlighted by the dotted line. The number of samples is as follows: LD group, 5′*MYO7A* in the treated eye, n = 6 at days 2, 8, and 31, and n = 2 at days 15 and 61; LD group, 3′*MYO7A* in the treated eye, n = 6 at days 2, 8, and 31, n = 4 at day 15, and n = 2 at day 61; LD group, 5′*MYO7A* in the untreated eye, n = 6 at days 2, 8, and 31, and n = 1 at day 61 (samples at day 15 could not be quantified due to incorrect PCR); LD group, 3′*MYO7A* in the untreated eye, n = 6 at days 2, 8, and 31, and n = 1 at day 61 (samples at day 15 were excluded due to incorrect PCR); HD group, 5′*MYO7A* and 3′*MYO7A* in the treated eye, n = 6 at days 2, 8, 15, and 31, n = 3 at day 61, and n = 1 at day 91; HD group, 5′*MYO7A* in the untreated eye, n = 6 at day 2, n = 5 at days 8 and 15, and n = 3 at days 31 and 61; HD group, 3′*MYO7A* in the untreated eye, n = 6 at days 2 and 15, n = 5 at day 8, n = 2 at day 31, and n = 3 at day 61; vehicle group, 5′*MYO7A*, n = 3 at days 2, 31, 61, and 91, n = 2 at day 8, and n = 4 at day 15; vehicle group, 3′*MYO7A*, n = 4 at day 2 and n = 3 at days 8, 15, 31, 61, and 91. Samples at day 91 of the LD group and of untreated eyes of the HD group were not analyzed.

outside of the injection bleb was found in 4 out of 8 (50%) and in 2 out of 10 (20%) eyes receiving the HD and the LD, respectively (Tables S11 and S12). Conversely, gray-white foci similar to Dalen-Fuchs nodules were found only in the LD-treated eyes (3 out 10 [30%]) at the end of the study in the injection site (IS) area (Tables S11 and S12). Recovery over time was observed in most cases. Overall, clear and consistent differences between groups were not appreciated in ophthalmic examinations. Table S13 explains the different gradings used for the ophthalmoscopic analysis.

No significant changes in intraocular pressure (IOP) were observed in eyes administered either with the LD or HD of dual AAV8.*MYO7A* compared with AAV vehicle-treated eyes (Table S14). Reduction in IOP compared with baseline levels was observed in some eyes soon after the surgical procedure (mainly at study days 2/3 and 5/6 [Table S14]). This lowering, likely attributable to inflammation, reverted over time.

Assessment of dual AAV8.*MYO7A*-related effects on NHP retinal and cortical function was based on dark-adapted (rod-mediated) and light-adapted (cone-mediated) electroretinography (ERG), and

for values above the limit of quantification, >LOQ, and in a decreasing order of MYO7A expression levels. The LOQ and LOD are 500 and 150 RNA copy number/μg of RNA, respectively. Samples above LOQ are represented as black circles, and samples below LOQ are represented as gray circles. The area under the LOQ is highlighted by the dotted line. L, left; R, right; LN, lymph node; LGN, lateral geniculate nucleus; Sup, superior. Samples for biodistribution and expression analyses were collected at week 13/14 post administration.

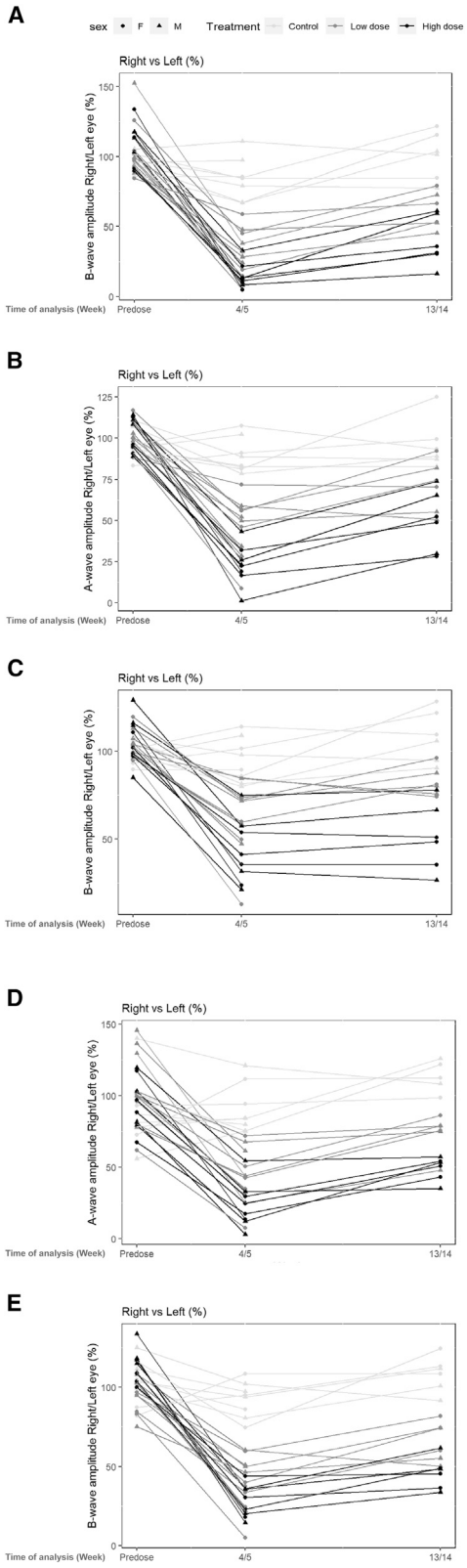

Figure 4. Subretinal administration of dual AAV8.*MYO7A* induced dose-dependent effects on NHP retinal electrical function that improve over time

Electroretinography was performed at predose, 4/5 weeks, and 13/14 weeks in CTR (light gray), LD (dark gray), and HD (black) groups. Representative scotopic (A–C) and photopic conditions (D and E) are reported. Results are reported for each single treated right eye as percentage of the contralateral untreated left eye. Males are indicated as circles and females as triangles. The number of eyes is as follows: CTR group, n = 8 at predose and week 4/5, and n = 6 at week 13/14; LD group, n = 12 at predose and week 4/5, and n = 6 at week 13/14; HD group, n = 8 at predose and week 4/5, and n = 6 at week 13/14.

visual evoked potentials (VEPs) recorded prior to dosing, at 4/5 weeks post injection (interim time point), and 13/14 weeks post injection (terminal time point). Values from animals in the three treatment groups were similar at predose evaluation. No changes in ERG and VEP were observed in AAV vehicle-treated right eyes, comparable with the fellow untreated (left) eye both at the interim and terminal time points (Figure 4; Tables S15 and S16).

Recordings collected at the interim time point showed that eyes administered with either LD or HD of dual AAV8.*MYO7A* had significant reductions in ERG amplitude (Figure 4; Tables S15 and S16). The ERGs from dual AAV8.*MYO7A*-treated eyes were generally less than 50% of the fellow eye's amplitude and were more reduced in HD-treated compared with LD-treated eyes (Figure 4; Tables S15 and S16). Oscillatory potentials were markedly reduced in both experimental groups (Table S15). Delay in cortical VEP at this time point was observed in 4 out of 12 (33%) LD-treated and 6 out of 8 (75%) HD-treated eyes, and more frequently in females than in males (Table S16).

Recordings performed at 13/14 weeks post injection showed that electrical responses in the LD group largely recovered, resulting in only a mild ERG reduction in this group (Figure 4; Tables S15 and S16). Specifically, 2 out of 6 LD-treated eyes at week 13/14 showed ERGs in the expected range while others still presented various degrees of reduction (Figure 4; Tables S15 and S16). Conversely, a modest or only partial recovery was observed in the HD group which still had markedly reduced ERG, whereas the latency of the VEP in this group generally improved with only one female still affected (Figure 4; Tables S15 and S16). Therefore, ERG findings were dose dependent overall and improved over time. Details on descriptive analysis and on the pairwise comparison are reported in Tables S15 and S16.

In vivo evaluation of the retinal structure was performed through optical coherence tomography (OCT) analysis. Retinal scanning showed common subretinal injection-related effects, including the presence of hyper-reflective foci/subretinal hyper-reflective material/hyper-reflective material (HRF/SHRM/HRM), thinning, disorganization, and discontinuity of the bacillary layer (photoreceptor layers and/or RPE), and mild posterior vitreous detachment close to the IS, i.e., within the bleb area, in all eyes administered with a subretinal injection of AAV vehicle (data not shown). Moreover, clusters of SHRM/HRM away from the IS and retinal thinning away and near to the IS were found in 1 out of 6 CTR eyes (Table 2).

Table 2. Incidence of uncommon OCT findings at 13/14 weeks post injection

Group	Increased HRF/SHRM/HRM	Mild RFNL thickening	Retinal thinning near IS	Cluster of SHRM away from IS	Area of retinal thinning away from IS
CTR	0/6	0/6	1/6	1/6	0/6
LD	6/6	2/6	4/6	1/6	0/6
HD	6/6	3/6	3/6	3/6	4/6

The number of eyes with OCT findings not related to surgical procedure (subretinal injection) observed at the end of the study is shown.
CTR, AAV vehicle group; LD, low-dose group; HD, high-dose group; HRF, hyper-reflective foci; SHRM, subretinal hyper-reflective material; HRM, hyper-reflective material; RFNL, retinal nerve fiber layer; IS, injection site.

In addition to findings associated with the surgical procedure, all eyes administered with dual AAV8.*MYO7A* had an increased number of HRF/SHRM/HRM compared with CTR eyes. Also, mild thickening of the retinal nerve fiber layer, likely related to inflammation, was observed in 2 out of 6 and 3 out of 6 eyes receiving the LD and HD, respectively, and areas of retinal thinning near to the IS (including outer nuclear layer thinning) were observed in 4 out of 6 and 3 out of 6 eyes receiving the LD and HD, respectively, while the incidence of these findings was 1 out of 6 in CTR eyes (Table 2). Conversely, areas of retinal thinning and clusters of SHRM/HRM away from the IS showed a comparable incidence between LD and CTR eyes, while the incidence was higher in the HD group (Table 2). Importantly, these alterations were not extended to the foveal region in any of the LD-treated eyes. Macula scans at 13/14 weeks post injection are comparable with predose scans (Figure S2). The photoreceptor nuclear layer (specifically the inner segment/outer segment line, also known as ellipsoid zone) and the inner retina had a normal appearance (Figure S2). Conversely, alteration of the foveal region was observed in all HD-treated eyes 13/14 weeks post injection, further confirming a dose-dependent toxicity, although some recovery occurred compared with 4/5 weeks post injection (Figure S2). Indeed, the ellipsoid zone or inner segment/outer segment line disappeared in HD-treated eyes at week 4/5 while it was again visible at week 13/14, suggesting this alteration improves over time (Figure S2).

Hyper-reflective material/spots were noted in the foveal region of HD-treated eyes at both time points, which is in line with the retinal inflammation reported in the histopathological analysis.

Specifically, no microscopic alterations were found in CTR-administered eyes except for RPE hypertrophy/hyperpigmentation near the IS of right eyes, with minimal retinal degeneration observed in one eye at the interim sacrifice (4/5 weeks) and in one eye at the terminal sacrifice (13/14 weeks; Figures 5A and 5B). Microscopic alterations were found in eyes administered with dual AAV8.*MYO7A*. Findings included RPE degeneration with hypertrophy, hyperpigmentation or loss of pigmentation, and loss or detachment of RPE cells, which sometimes transmigrate through the retina. RPE degeneration was often associated with degeneration of the overlying/adjacent neuroretina, which was characterized by loss of outer segments of the photoreceptors to a more extensive disorganization and loss of primarily outer retinal layers; in general, areas of more severe retinal degeneration were associated with areas of increased severity of RPE degeneration.

Other findings included: (1) retinal inflammation, which ranged from perivascular cuffing of inflammatory cells at a minimal severity to transmigration of inflammatory cells throughout all retinal layers at a slight severity; (2) multifocal choroidal inflammation, which was observed close to a more severely affected area of RPE/retina degeneration; and (3) vitreous inflammation. Inflammatory cells were represented by lymphocytes and plasma cells. Importantly, findings were more severe in animals sacrificed at interim time points compared with animals sacrificed at the end of the study, further supporting the indication of a possible recovery over time, as also indicated by ERG and OCT improvements (Figures 4 and S2; Tables S15 and S16). Accordingly, microscopic findings were generally dose-dependent in terms of grade of severity (Figures 5A and 5B). At the end of the study, RPE degeneration was moderate (3 out of 6) to slight (3 out of 6) in the LD-treated eyes and marked (1 out of 4) to moderate (3 out 4) in the HD-treated eyes, while retina degeneration was slight (4 out of 6) to minimal (2 out 6) in the LD-treated eyes and moderate (2 out of 4) to slight (2 out of 4) in the HD-treated eyes (Figure 5A). Similarly, inflammation was minimal or absent in LD-treated eyes, while minimal to slight inflammation was found in the HD-treated eyes at the end of the study (Figure 5B). Overall, microscopic alterations reflect the dose-dependent ERG reduction, with HD-treated eyes being more impacted than LD-treated eyes.

All other microscopic findings were considered spontaneous and/or incidental because they occurred at a low incidence, were randomly distributed across groups (including controls), and/or their severity was as expected for cynomolgus monkeys of this age (data not shown). Specifically, no findings attributable to dual AAV8.*MYO7A* were noted in the non-ocular tissues (data not shown).

We did not observe any alteration in blood clinical chemistry (Table S17) or body weight (Table S18 and S19) due to dual AAV8.*MYO7A* subretinal administration. Similarly, no changes in urinalysis (Table S20 and S21) or hematology analysis (Table S22) were detected, except for the animals sacrificed at interim where test results included minimal to mild decreases in red cell mass (i.e., red blood cell count, hemoglobin concentration, and/or hematocrit) and minimally increased absolute reticulocyte count. These differences may have been related to previous blood collections for other tests. Necropsy was performed at the termination of the study and at an interim time point. No macroscopic differences or organ weight differences were found that could be attributed to dual AAV8.*MYO7A* (data not shown).

Immune responses following subretinal administration of dual AAV8.*MYO7A* in NHPs

All NHPs in the study (including animals administered with AAV vehicle) except two designated to the HD group (P0202 and P0503) were seropositive to AAV8 at predose (Table S23). NHPs treated

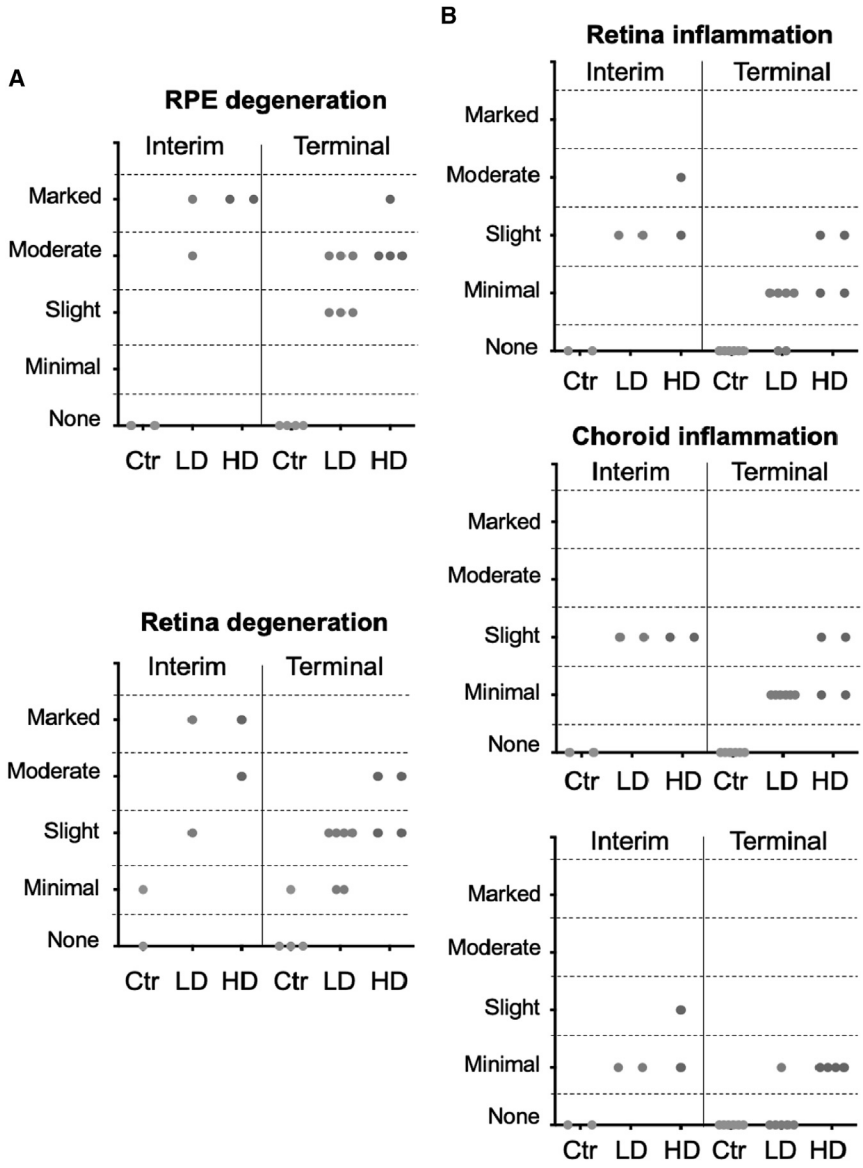

Figure 5. Microscopic findings following subretinal administration of dual AAV8.*MYO7A* in NHPs

(A) Severity scoring of retinal pigment epithelium (RPE) and retina degeneration. Each dot represents a single eye. Histopathology was performed either at interim (6–9 weeks post injection) or at the terminal time point of analysis (13–14 weeks post injection). CTR, eyes administered with AAV vehicle; LD, eyes administered with low dose; HD, eyes administered with high dose. (B) Severity scoring of retina, choroid, and vitreous inflammation. Degrees of severity are defined as follows: minimal describes an inconspicuous change; slight refers to a noticeable but not prominent feature; moderate describes a prominent feature; marked refers to a dominant but not overwhelming feature; severe implies an overwhelming condition.

with AAV vehicle did not show an increase in neutralizing antibodies (Nabs) to AAV8 except one (P0002), which had a possible natural infection of wild-type AAV8 (Figure 6A and Table S23). Animals receiving subretinal administration of dual AAV8.*MYO7A* showed increase of Nabs regardless of the dose, as expected and reported by others (Figure 6A and Table S23).[24,25] While no correlation was found between levels of Nabs to AAV8 and ocular alterations, we observed a further increase in Nab levels in 5 out of 6 (>80%) animals in the HD group between 5 weeks and 13/14 weeks post injection (Figure 6C and Table S23). Animals in the LD group showed a different trend, with 7 out of 10 (70%) animals having stable or reduced levels of Nabs to AAV8 and only 3 out of 10 (30%) animals having increased Nab levels (Figure 6B and Table S23). Additionally, the HD group showed a 115-fold increase in Nab titer 5 weeks post injection compared with baseline, whereas the increase was 54-fold in the LD group (Figure 6A and Table S23). Anti-AAV8 serum immunoglobulin G (IgG) but not IgM levels increased after subretinal administration of dual AAV8, as expected, since a natural AAV infection occurred before treatment (Table S23). Stable IgM levels were also observed in the two naive macaques in the HD group; this may be explained by either a natural AAV infection which occurred after collection of the predose serum sample or an IgM-to-IgG seroconversion which occurred earlier than the 5-weeks time point of analysis (Table S23).

We measured cell-mediated immune responses against AAV8 in 2 out of 9 LD and 4 out of 8 HD animals (Table S24). No CTR animal had cellular immune responses to AAV8. Finally, while no antibodies to human MYO7A were detectable in NHPs serum (data not shown), we measured cellular immune responses to the transgene product in 4 out of 9 LD macaques and 4 out of 9 HD macaques (Table S24). Autoreactive cells were measured in some animals in the CTR (5 out of 8), LD (4 out of 9), and HD (2 out of 8) groups.

DISCUSSION

In this work, we produced data required for the clinical translation of a gene therapy based on subretinal administration of dual hybrid AAV vectors serotype 8 encoding human *Myosin VIIA* (dual AAV8.*MYO7A*) to treat RP associated with USH1B. To the best of our knowledge, this represents the first report on the use of dual AAV vectors in the primate retina.

The dual AAV8.*MYO7A* lot used in this work was produced according to a process that is similar to the GMP process employed for the clinical lot. The dose-response study in sh1$^{-/-}$ mice allowed selection of

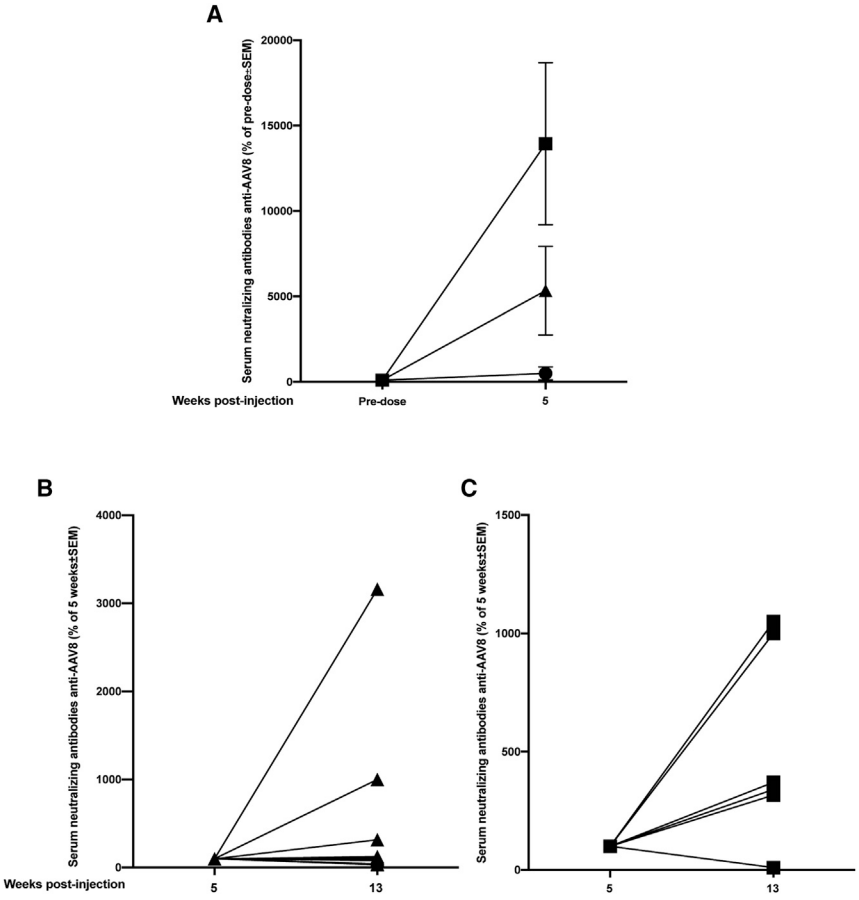

Figure 6. Serum levels of neutralizing antibodies to AAV8 capsid following subretinal administration of dual AAV8.*MYO7A* in NHPs

Serum neutralizing antibodies (Nabs) to AAV8 were measured by an inhibition transduction assay predose and at 5 and 13 weeks post injection. Nab titer was calculated as the reciprocal of the highest serum dilution that inhibited AAV transduction by ≥50% compared with the control without serum (100% transduction). (A) Nab titers measured at 5 weeks post injection are presented as percentage of predose and are shown as mean ± SEM for animals administered with AAV vehicle (circles), LD (triangles), and HD (squares) of dual AAV8.*MYO7A*. (B and C) Nab titer measured at 13 weeks post injection for each animal receiving LD (B, triangles) or HD (C, squares) of dual AAV8.*MYO7A* are presented as percentage of the corresponding Nab titer measured at 5 weeks post injection.

three dual AAV doses that induce dose-dependent MYO7A expression and improve melanosome localization in the RPE of the sh1 mouse model of USH1B. Since sh1 mice, like other rodent models of Usher syndrome, do not present with the progressive photoreceptor degeneration observed in humans,[26] we need to rely on ultrastructural retinal abnormalities such as RPE melanosome mislocalization[9,17] to infer the biological impact of our therapeutic approach. While this is of course limiting in terms of prediction of the therapeutic effect in humans, we show that the three doses of dual AAV we administered subretinally in mice results in expression of MYO7A protein between 40% and 67% of that detected in heterozygous sh1$^{+/-}$ mice. Considering that the AAV transduced retinal area in mice is about 30% of the total retina, and that the western blot analysis is performed using a whole retinal lysate (which therefore includes about 70% of untransduced tissue), in the transduced area we likely achieve between 60% and 100% of the total MYO7A content of a wild-type mouse (assuming that heterozygous sh1$^{+/-}$ mice produce 50% of the levels of MYO7A of wild-type sh1$^{+/+}$ mice). If this holds true in humans, we are reconstituting levels of MYO7A expression expected to be therapeutically relevant even at the low and intermediate doses of dual AAV.

The biodistribution study in NHPs shows that dual AAV vectors remain mostly localized to the retina and few other ocular tissues upon subretinal administration, while spreading to extraocular components of the visual pathway was negligible. Biodistribution to systemic tissues was minimal. Data suggest that vector spreading occurred through serum and the lymphatic system; no dual AAV DNA was found in gonads, which minimizes the risk of germline transmission. These results are in line with a previous study based on subretinal injection of similar AAV8 doses in NHPs.[22] Similarly, MYO7A expression was mainly confined to the retina. In any case, ectopic expression of dual AAV8.*MYO7A* should not be worrisome considering the wide expression profile reported for MYO7A RNA (https://www.proteinatlas.org; https://www.ncbi.nlm.nih.gov/ gene ID: 4647).

Vector shedding in tears and serum was transient and similar in duration to what was previously reported in NHPs receiving similar doses of AAV8.[22] Similarly, no AAV8 vector shedding in tears was demonstrated in subjects enrolled in a recent gene therapy clinical trial (ClinicalTrials.gov identifier: NCT02610582[2]). Overall, the dual AAV8.*MYO7A* pharmacokinetic profile appears safe.

Dual AAV8.*MYO7A* subretinal administration to NHP resulted in AAV dose-dependent ocular structural and functional findings, which were mild at the ld and improved over time. The observed amelioration suggest that these alterations may be attributed to an inflammatory process, likely caused by AAV, as suggested by our immunology data and results of non-clinical studies using subretinal administration of similar AAV8 doses in NHPs.[27] In that study from Reichel et al., a role for AAV8-induced inflammatory responses was suggested by the presence of mononuclear cell infiltrates (identified as CD8$^+$ T cells and CD20$^+$ B cells in the AAV8-injected areas), as well as hyper-reflective spots and reversible changes in the ellipsoid zone (EZ) signal in the OCT analysis. Importantly, the corresponding

GMP lot of that vector was used in a clinical trial for achromatopsia (ClinicalTrials.gov identifier: NCT02610582) and showed a good safety profile in humans.[2] Notably, EZ changes are typically observed in eye inflammatory diseases and seem to be associated with an alteration of refractive characteristics of photoreceptors rather than with their disruption;[28] indeed, as inflammation resolves the EZ reappears, thus excluding a permanent loss of cells or their function. The EZ findings reported in the study from Reichel et al.[27] resemble what we observed in the macula region of HD-treated eyes, where the EZ line reappears at week 13/14 compared with week 4/5, albeit improvement was partial. Also, the presence of persistent HRF in the bleb areas was reported in NHPs studies, based on subretinal injections of AAV8 at similar doses.[29] Notably, HRF were described in three different retinal gene therapy trials and were easily managed with corticosteroids.[2,6,30] Although our GLP study did not identify a no observed adverse event level (NOAEL), overall data suggest that the LD of dual AAV8.*MYO7A* is close to the NOAEL. Considering that the LD administered in NHPs corresponds to 1.6-times the highest dose of the clinical trial (based on the different retinal areas between the two species), we do not plan to change the doses proposed for the clinical trial and defined them on the basis of the dose-response study in sh1 mice. Importantly, the clinical trial is a dose-escalation study in which safety must be assessed before treatment of the next subject in each dose cohort and before dose escalation. Therefore, we believe that the clinical study design and the unmet medical need represented by USH1B RP result in a positive risk/benefit ratio and pave the way for the use in humans of dual AAV8.*MYO7A*.

MATERIALS AND METHODS

Generation of AAV vector plasmids

Dual AAV vector plasmids (5′ and 3′ plasmids) used for AAV vector production were generated as previously described.[9] Both plasmids contain the ITRs of AAV serotype 2. The 5′ plasmid contained the cytomegalovirus (CMV) enhancer and a shortened version of the chicken β-actin (CBA) promoter to drive MYO7A expression in both RPE and photoreceptors where MYO7A is expressed.[17,31,32] We added a modified version of the simian virus 40 promoter's intron (SV40),[33] followed by the N-terminal portion of the human *Myosin VIIA* (*MYO7A*) and a splice donor (SD) sequence. The 3′ plasmid contained a splice acceptor sequence (SA) and the C-terminal portion of the transgene coding sequence (CDS) followed by the bovine growth hormone polyadenylation signal. The *MYO7A* CDS was split at a natural exon-exon junction, between exons 24 and 25 (5′ half: NM_000260.3, bp 273–3,380; 3′ half: NM_000260.3, bp 3,381–6,920).

The recombinogenic sequence contained in the hybrid AK vector plasmids is derived from the phage F1 genome (accession number GenBank: J02448.1; bp 5,850–5,926).[9]

AAV vector production and characterization

A single dual AAV8.*MYO7A* lot was used in the non-clinical safety and dose-response studies. Dual AAV8.*MYO7A* is a mixture in a 1:1 ratio of two AAV vectors serotype 8 (AAV8) containing the 5′-half sequence of human *MYO7A* coding sequence (AAV8.5′*MYO7A*, vector 1) and the 3′-half sequence of human *MYO7A* coding sequence (AAV8.3′*MYO7A*, vector 2). AAV8.5′*MYO7A* and AAV8.3′*MYO7A* vectors were produced by the Telethon Institute of Genetics and Medicine (TIGEM) AAV Vector Core (Pozzuoli, Italy) and by ReiThera (Castelromano, Italy) through a process that was similar to the good manufacturing process used for clinical production and based on triple transfection of human embryonic kidney 293 cells expressing the SV40 large T antigen (HEK293T), followed by two rounds of $CsCl_2$ purification.[34–38]

The physical titer of each vector [genome copies(GC)/mL] was determined by TaqMan quantitative PCR (qPCR) (Applied Biosystems, Waltham, MA). Primers and probes were designed to anneal on 5′*MYO7A* for AAV8.5′*MYO7A* and BGH pA for AAV8.3′*MYO7A*. The final drug product (DP), i.e., dual AAV8.*MYO7A*, was then generated by mixing vector 1 and vector 2 in a 1:1 ratio, followed by: (1) dilution in the formulation buffer (referred to as AAV vehicle), which is PBS (Thermo Fisher Scientific, Waltham, MA) supplemented with 35 mM sodium chloride (Sigma-Aldrich, St. Louis, MO) and 0.001% poloxamer 188 (P188, Sigma-Aldrich); and (2) sterile filtration post-filtration physical titer determined in the final DP.

Quality control was performed on this lot to assess sterility, purity, potency, and potential process-related and product related impurities. Main results are reported in Table S1. This lot was shipped to the LabCorp (Madison, WI) test facility and to TIGEM.

Test facility, test sites, and animals

Pigmented shaker1$^{4626SB/4626SB}$ (referred to as sh1$^{-/-}$) mice were used in the dose-response study. Sh1 mice used in this study were either affected (sh1$^{-/-}$) or unaffected (sh1$^{+/-}$). Mice were housed at the TIGEM animal house (Pozzuoli, Italy) and maintained under 12:12-h light/dark cycle, and collected eyecup samples were analyzed at TIGEM and the Federico II University Department of Translational Medicine Medical Genetics Laboratory. Genotyping was performed as previously described.[9] The study was carried out in accordance with both the Association for Research in Vision and Ophthalmology Statement for the Use of Ophthalmic and Vision Research and with the Italian Ministry of Health regulation for animal procedures (Ministry of Health authorization numbers: 147/2015-PR and 301/2020-PR).

Twenty-eight (14 males and 14 females) adult (age 24–36 months) cynomolgus macaques (*Macaca fascicularis*) were used to assess the safety, biodistribution, and expression of dual AAV8.*MYO7A* following subretinal administration. The study was performed according to the United States Food and Drug Administration GLP for Nonclinical Laboratory Studies (Code of Federal Regulations, Title 21, Part 58) and OECD principles. NHPs were housed at LabCorp, which is fully accredited by the Association for the Assessment and Accreditation of Laboratory Animal Care. All procedures were in compliance with the applicable animal welfare acts and were approved by

the local Institutional Animal Care and Use Committee. Animals placed in the study were selected on the basis of available results from pretest examinations (e.g., body weights, food consumption, clinical observations, and clinical pathology) and were assigned to dose groups based on predose cage positions/cage mates. Eight NHPs (4 males and 4 females) received a subretinal administration of AAV vehicle (CTR), while 12 NHPs (6 males and 6 females) and eight NHPs (4 males and 4 females) received a subretinal administration of the LD and HD of dual AAV8.*MYO7A*, respectively. Right eyes were treated, while contralateral (left) eyes were left untreated as controls. Samples of the GLP study were analyzed at LabCorp, Genethon (Evry, France), and Genosafe (Evry, France). *In vivo* safety evaluations were performed at LabCorp.

Vector formulation and administration

An equal volume (1.1 μL) of either dual AAV8.*MYO7A* or AAV vehicle was delivered subretinally in mice via a posterior trans-scleral transchoroidal approach.[39] Dual AAV8.*MYO7A* was administered undiluted or serially diluted in AAV vehicle to administer from 1.37E+10 (undiluted) to 4.4E+9 (1:3.13 dilution) to 1.37E+9 (1:10 dilution) total GC/eye.

Dual AAV8.*MYO7A* administered in NHPs was diluted 1:2.7 in AAV vehicle to reach a dose of 1.37E+12 total GC/eye (LD) in a total volume of 300 μL. An undiluted dose of dual AAV8.*MYO7A* was tested to reach a higher dose of 3.75E+12 total GC/eye (HD). The macaque retinal area is 1.6-times smaller than that of humans; therefore, doses tested in the safety study are respectively 1.6- and 4.3-times higher than the highest dose proposed for the clinical trial.[18,19] The subretinal administration in cynomolgus macaques was performed through an anterior trans-scleral approach following a pars plana vitrectomy using a Dutch Ophthalmic Research Center (Zuidland, the Netherlands) subretinal injection device (41-gauge subretinal injection needle, 23-gauge/0.6 mm, Ref. 1270 EXT). Both dual AAV8.*MYO7A* and the AAV vehicle control were administered in the right eye of each non-human primate in a total volume of 300 μL and delivered to the perimacula as two blebs of 150 μL each, one in the superior retina and one in the inferior retina. The injection procedure was performed by a vitreoretinal surgeon assisted by a board-certified veterinary ophthalmologist from LabCorp. A medication regimen was started 3 days before dosing to minimize surgery-related inflammation and/or infection. Specifically, oral prednisolone was administered as follows.

- 1 mg/kg/die for 10 days, starting on day −3 up to day 7.
- 0.5 mg/kg/die for 7 days, starting on day 8 up to day 14.

  Also, Neo-Poly-Dex ointment (containing the corticosteroid dexamethasone) was topically applied on day −1 (day before dosing), day 1 (dosing day), and days 2 and 3.

Western blot analysis

Eyes from pigmented sh1 mice (+/− or −/−) were enucleated 5 weeks following the AAV injection, respectively, and lysed in RIPA buffer (50 mM Tris-HCl [pH 8.0], 150 mM NaCl, 1% NP-40, 0.5% Na-deoxycholate, 1 mM EDTA [pH 8.0], 0.1% SDS). Lysis buffer was supplemented with 0.5% phenylmethylsulfonyl fluoride (Sigma-Aldrich) and 1% complete EDTA-free protease inhibitor cocktail (Roche, Basel, Switzerland). Protein concentration was determined using Pierce BCA protein assay kit (Thermo Fisher Scientific). After lysis, samples were denatured at 99°C for 5 min in 4× Laemmli sample buffer (Bio-Rad, Hercules, CA) supplemented with β-mercaptoethanol (Sigma-Aldrich) diluted 1:10. Samples were separated on 4%–20% gradient precast TGX gels (Bio-Rad). The following antibodies were used for blotting: custom anti-MYO7A (1:200, polyclonal; Primm, Italy) that recognizes a peptide corresponding to amino acids 941–1,070 of the human MYO7A protein anti-dysferlin (1:500, MONX10795; Tebu-Bio, Le-Perray-en-Yvelines, France). The quantification of western blot bands was performed using ImageJ software. Myosin VIIA expression was normalized over the expression of dysferlin. For each gel, two different eye lysates of unaffected $sh1^{+/-}$ were loaded and quantified, and the average value was used to calculate MYO7A expression levels of test samples loaded in the same gel.

Melanosome localization analysis

Eyes from pigmented sh1 mice (+/− or −/−) were enucleated 3 months following the AAV injection and cauterized on the temporal side of the cornea. Fixation was performed using 2% glutaraldehyde (Electron Microscopy Sciences, Hatfield, PA) and 2% paraformaldehyde (Electron Microscopy Sciences) in 0.1 M PBS overnight, rinsed in 0.1 M PBS, and dissected under a light microscope. The temporal portions of the eyecups were embedded in Araldite 502/Embed 812 (Electron Microscopy Sciences). Semi-thin (0.5 μm) sections were transversally cut on a Leica Ultramicrotome RM2235 (Leica Microsystems, Wetzlar, Germany), mounted on slides, and stained with 1% toluidine blue (Carlo Erba, Milan, Italy) with 2% borace staining (Thermo Fisher Scientific) in deionized water. Melanosomes were counted by a masked operator in a montage of the entire retinal section obtained through acquisition of overlapping fields using a Zeiss Apotome (Carl Zeiss, Oberkochen, Germany) with 100× magnification; the entire retinal section was then reconstituted on Photoshop software (Adobe, Mountain View, CA). Melanosome counts and RPE measurements were performed using ImageJ software. Melanosome number was normalized over the length of the RPE divided by 100 μm.

TaqMan qPCR-based biodistribution and shedding analysis in NHPs

Since the target organ of dual AAV8.*MYO7A* is the eye and AAV vectors are not expected to spread to non-ocular tissues following subretinal injection,[20–23] biodistribution was focused on ocular tissues and components of the visual pathway, and only a subset of systemic non-ocular tissues was instead investigated.

- Retina: two 6-mm punches of full-thickness retina (neuroretina through sclera) were collected from each eye. For the treated (right) eye, one was from a bleb area and one from non-bleb area. For the untreated (left) eye, punches were collected from corresponding areas of the retina

- Eye: right and left optic nerve, ocular muscle, vitreous fluid, lens, and anterior segment
- Brain: optic chiasm, right and left lateral geniculate nucleus (LGN), superior colliculus, optic tract, occipital cortex, thalamus, and cerebellum
- Non-ocular tissues: heart, jejunum, kidney, liver, lung, mandibular lymph node, mesenteric lymph node, parotid lymph node (left or right, as applicable), muscle (biceps femoris), pancreas, spleen, ovary or testis, and epididymis

Vector shedding was evaluated in tears and serum. Total DNA was isolated using the following kits: NucleoSpin Tissue or NucleoBond AX (Macherey-Nagel, Düren, Germany) for tissues, and NucleoSpin Blood QuickPure (Macherey-Nagel) or the QIAamp DNA Blood Kit (QIAGEN, Hilden, Germany) for blood. DNA was quantified by measuring the optical density (OD) at 260 nm using a spectrophotometer (PowerWave XS; BioTek [now Agilent], Santa Clara, CA) to normalize the amount of DNA. Tears and serum are expected to not have quantifiable genomic DNA; therefore, normalization of these samples was not performed. DNA samples were analyzed by qPCR, using the QS7 real-time PCR system (Applied Biosystems). The following primers and TaqMan probe (Applied Biosystems) designed for the 5′*MYO7A* and 3′*MYO7A* were used to detect AAV8.5′*MYO7A* DNA and AAV8.3′*MYO7A* DNA, respectively:

5′*MYO7A* forward primer [Fw], CTA CGC ACT CCT ACA CC (600 nM)

5′*MYO7A* reverse primer [Rev], ACC TGT CTT GTA ACC TTG A (900 nM)

5′*MYO7A* TaqMan MGB probe, CCA CTG CTC TAC CAT GAC GAC GA (100 nM)

3′*MYO7A* Fw, CTT CCT ACA TTA GCC AGA TG (900 nM)

3′*MYO7A* Rev, GAG GCA GAT CTC GAA GAC (900 nM)

3′*MYO7A* TaqMan MGB probe, ACA GCC ATG AGC AAA CAG CG (100 nM)

The LOQ of the assay was 50 GC/μg DNA as recommended by Food and Drug Administration guidelines (ICHQ2(R1)). This limit corresponds to the lowest number of vector copies that was reliably measured in 1 μg of host DNA with repeatability, intermediate precision, and measured bias less than 10% of variability. The LOD was 15 GC/μg DNA corresponding to an LOQ × 3/10, with LOQ = 10× background noise and LOD = 3× background noise (background noise <5 GC/μg DNA).

Since the range of quantification was from 20E+8 to 10E+8, the LOQ and LOD were 20 GC/well (corresponding to the lowest amount of vector GC in the standard curve) and 6 GC/well, respectively, in body fluids where no host DNA was quantified. The normalized target quantity is reported as the number of GC per 100 μL of fluid. When less than 400 ng host DNA or less than 90 μL for fluids was used, these limits were recalculated as follows: for tissues, 400 ng/analyzed quantity × LOQ (50) or LOD (15). For fluids, LOQ was recalculated according to the following formula: (LOQ × 100 μL)/(volume of sample tested/6). LOD was recalculated according to the following formula: (LOD × 100 μL)/(volume of sample tested/6), where 6 is the ratio between the volume of eluted sample (90 μL) and the volume tested by qPCR (15 μL). The PCR assay acceptance criteria were the following:

- Efficiency I (E): $90\% \leq E \leq 110\%$
- Correlation coefficient for the reference range: $R^2 \geq 0.99$
- No significant detection (copy number < LOD) for negative controls.

Inhibition was assessed by monitoring the number of copies of an endogenous reference (i.e., macaque albumin gene) compared with a set range (for tissues, total blood, and stools) or by adding a number of known copies of the reference plasmid before extraction (for plasma).

TaqMan qRT-PCR-based expression analysis

Tissue samples dedicated to RNA extraction were maintained in RNAlater (Sigma-Aldrich). Retina samples were collected as described in the previous paragraph. After being left overnight at 4°C, RNAlater was removed and tissue samples were stored at −80°C. Total RNA was then isolated only from tissues that resulted positive to both AAV8.5′*MYO7A* DNA and AAV8.3′*MYO7A* (Figure 2A) using a Nucleospin RNA kit (Macherey-Nagel). Quantification and RNA integrity were checked using the Experion electrophoresis system (Bio-Rad). Retrotranscription was performed using Superscript VILO Master Mix (Invitrogen, Waltham, MA) on 200 ng of RNA (in triplicate) spiked with 1E+04 copies of RNA of the *Arabidopsis thaliana* exogenous gene (RBCL) to identify any potential inhibition of qRT-PCR reactions; when less than 200 ng RNA was extracted, the maximum amount of RNA was reverse transcribed. The following primers and TaqMan probe (Applied Biosystems) were designed to amplify a region of human MYO7A around the splitting point of dual AAV8.*MYO7A*:

Fw (350 nM), 5′-CTG AGT ATA AAT TTG CCA AGT TCG CG-3′

Rev (350 nM), 5′-CAC AGG GAT CTT CTC ACT GCC A-3′

TaqMan MGB probe (250 nM), 5′-TAC TTG GGC TCA GGG AGG TCC CCC ATG A-3′

LOQ and LOD were assessed based on a previous study that we conducted on NHPs injected with dual AAV8.*MYO7A* (RD.046/19) and were set at 500 and 150 RNA copy number/μg of RNA, respectively.

A synthetic RNA corresponding to the target sequence was used to prepare a standard curve ranging from LOQ to 10E+7 RNA vector copies.

The PCR assay acceptance criteria were the following:

- Efficiency I (E): 80% $\leq$ E $\leq$ 105%
- Correlation coefficient for the reference range: $R^2 \geq 0.98$
- No significant detection (copy number < LOD) for negative controls
- All the samples, controls, and range concentrations analyzed by qPCR were tested in triplicate

Safety assessments in NHPs

Ocular toxicity was evaluated by a board-certified veterinary ophthalmologist and was based on ophthalmic examinations with a slit-lamp biomicroscope in conjunction with an indirect ophthalmoscope, IOP measurements, and assessment of full-field ERG parameters, as well as evaluation of scan images obtained using OCT. Analyses were conducted on eyes previously dilated with a mydriatic agent and on animals anesthetized with 0.5% proparacaine. Systemic organ-specific toxicity was assessed by evaluation of electrocardiography, clinical hematology, and urine analysis as well as anatomic pathology endpoints, including necropsy and histopathology of ocular- and non-ocular tissues (brain, heart, jejunum, kidney, liver, lung, mandibular lymph node, mesenteric lymph node, parotid lymph node, muscle [biceps femoris], optic nerve, ovary, pancreas, spleen, and testis). Organ weights were evaluated exclusively in animals terminated at the end of the study (scheduled sacrifice). Pair organs were weighed together. Samples for histopathology were collected in modified Davidson's fixative for 48–96 h and subsequently transferred in 10% neutral-buffered formalin. Samples were then processed in 95% ethanol before embedding in paraffin. Sections (6–7 μm thick) analyzed for microscopic alterations were stained with H&E. Since simultaneous collection of ocular tissues for histopathology and biodistribution/expression analysis could not be performed, different macaques were designated to either ocular histopathology or biodistribution/expression at sacrifice, as shown in Table S25.

Immune response study in NHPs

Levels of anti-AAV8 Nab in NHP serum were measured with an *in vitro* reporter system. 2V6.11 cells were seeded in 96-well plates (2E+4 cells/well) and incubated in DMEM with 10% fetal calf serum (Life Technologies, Carlsbad, CA) at 37°C and 5% CO_2 for 24 h in the presence of ponasterone A (Life Technologies). Recombinant AAV8-CMV-luciferase (AAV8-CMV-Luc) was diluted in serum-free DMEM (Life Technologies) and incubated with semi-log serial dilutions (1:1–1:3,160) of the serum samples, then incubated for 1 h at 37°C. Subsequently, the serum-vector mixtures were added to the 2V6.11 cells, and after 24 h cells were lysed with the Bright Glo system (Promega, Madison, WI) and the luciferase activity measured on a luminometer (ENSPIRE, PerkinElmer, Waltham, MA). The neutralizing titer was reported as the highest serum dilution that inhibited AAV transduction by $\geq$50% compared with the control without serum (100% transduction). Samples were tested in duplicate.

IgG and IgM against AAV8 were measured with an ELISA assay in 96-well Nunc polysorp immunoplates (Dutscher, Bernolsheim, France) coated with rAAV to a final concentration of 1 μg/mL (which represents approximately 5.108 vector genomes/well). A standard curve made of purified human IgG or IgM (Interchim, Montluçon, France) was added directly to the plates. Plates were coated overnight at 4°C. The next day, after a blocking step, serum samples were added at dilution of 1:10 and 1:100 in duplicate and incubated for 1 h at 37°C. A horseradish peroxidase-conjugated monoclonal antibody specific for human IgG or IgM (Southern Biotech, Birmingham, AL) was added to the plates and incubated for 1 h at 37°C. The enzymatic reaction was developed with substrate solution 3,3′,5,5′-tetramethylbenzidine (Becton Dickinson, Franklin Lakes, NJ). The reaction was stopped with H_2SO_4 3 M solution, and OD measurements were done at 450 nm using a microplate reader (ENSPIRE, PerkinElmer). Anti-AAV IgG or IgM concentration was determined against the specific standard curve using 4-parameter regression, and results were expressed as μg/mL of Ig.

IgG against human MYO7A was detected by simple western blot (Protein Simple [Bio-Techne, Minneapolis, MN]). Protocol used was included in the kits, and test serum was diluted 1:10.

Reactive cells against AAV8 or human MYO7A were detected using an interferon-γ (IFN-γ) ELISpot assay. Peripheral blood mononuclear cells or splenocytes from NHPs were stimulated for 24 h with antigens derived from the vector's capsid or transgene. Specificity of the assay was controlled by a negative control, unstimulated cells (no antigen). At the end of the stimulation period, spots were revealed using a single-color enzymatic detection to analyze secretion of one cytokine (IFN-γ) and quantify spots forming cells.

Statistical analysis

Melanosome counts and MYO7A expression measurements in sh1 mice were compared with one-way ANOVA followed by the Tukey post hoc test. Comparisons of ERG parameters between treatment groups were performed by using Mood's median test plus multiple comparisons. Regarding chemical analysis, blood tests, urinalysis, and body and organ weight, comparison between treatment groups was performed using ANOVA followed by Dunnett's test or the Kruskal-Wallis rank-sum test, as appropriate. All results are reported as means ± SD or means ± SEM, except for ERG parameters shown as medians. The tests are two sided unless otherwise specified, and the level of significance is 0.05.

DATA AVAILABILITY

The authors confirm that the data supporting the findings of this study are available within the article and/or its supplemental information.

SUPPLEMENTAL INFORMATION

Supplemental information can be found online at https://doi.org/10.1016/j.omtm.2023.02.002.

ACKNOWLEDGMENTS

This research was supported by grants from the European Union Horizon 2020 (grant 754848) and the Italian UniNA and "Compagnia di

San Paolo" Star Plus 2020 Established Principal Investigator (grant 21-UNINA-EPIG-007). The authors would like to acknowledge Ivana Trapani for helpful discussions and feedback. Furthermore, we would like to thank Antonella Iuliano and Eugenio Del Prete from the TIGEM Bioinformatic core for statistical analysis of the experiments in Figure 1. Finally, we would like to thank Edoardo Nusco for his support with shaker1 animal handling and anesthesia. Graphical abstract and Figures 1A and 2C were created with BioRender.com (accessed on 1 November, 2022, 20 December, 2022 and 4 September, 2022, respectively). We would like to thank Phoebe Ashley Norman for her valuable support in English language editing.

AUTHOR CONTRIBUTIONS

R.F., F.D.A., and A.A. wrote the manuscript. R.F. and A.A. conceived, designed, and supervised the studies. F.D.A. performed the dose-response experiment in shaker1 mice. M.D., M.F., A.N., F.G., V.A., and S.C. produced and characterized the dual AAV8.*MYO7A*. F.T., P.M., and F.S. contributed to the analysis of the ocular findings including ERG, OCT, and histopathology. C.I. and E.M.S. performed subretinal injection in shaker1 mice. G.R., S.G., and M.G.V. performed the statistical analysis of safety study results in NHPs. N.T., P.R.l.B., and P.V. performed the immune response analyses. J.-B.M. performed the biodistribution and expression analyses.

DECLARATION OF INTERESTS

A.A. is Scientific Founder and Chief Scientific Officer of AAVantgarde BIO Srl, a company that has licensed dual AAV8.*MYO7A* and is further developing this program into the clinic. R.F. is currently an employee of AAVantgarde BIO Srl. J.-B.M. is an employee of Genosafe, a contract research organization involved in the further development of this program into the clinic. M.F., A.N., F.G., and V.A. are employees of Reithera Srl, a contract development and manufacturing organization involved in the further development of this program into the clinic. S.C. is Scientific Founder and Chief of Technology of Reithera Srl.

REFERENCES

1. (2018). FDA approves hereditary blindness gene therapy. Nat. Biotechnol. *36*, 7.
2. Fischer, M.D., Michalakis, S., Wilhelm, B., Zobor, D., Muehlfriedel, R., Kohl, S., Weisschuh, N., Ochakovski, G.A., Klein, R., Schoen, C., et al. (2020). Safety and vision outcomes of subretinal gene therapy targeting cone photoreceptors in achromatopsia: a nonrandomized controlled trial. JAMA Ophthalmol. *138*, 643–651. https://doi.org/10.1001/jamaophthalmol.2020.1032.
3. Lam, B.L., Davis, J.L., Gregori, N.Z., MacLaren, R.E., Girach, A., Verriotto, J.D., Rodriguez, B., Rosa, P.R., Zhang, X., and Feuer, W.J. (2019). Choroideremia gene therapy phase 2 clinical trial: 24-month results. Am. J. Ophthalmol. *197*, 65–73. https://doi.org/10.1016/j.ajo.2018.09.012.
4. Yu-Wai-Man, P., Newman, N.J., Carelli, V., Moster, M.L., Biousse, V., Sadun, A.A., Klopstock, T., Vignal-Clermont, C., Sergott, R.C., Rudolph, G., et al. (2020). Bilateral visual improvement with unilateral gene therapy injection for Leber hereditary optic neuropathy. Sci. Transl. Med. *12*. eaaz7423–11. https://doi.org/10.1126/scitranslmed.aaz7423.
5. Rakoczy, E.P., Magno, A.L., Lai, C.M., Pierce, C.M., Degli-Esposti, M.A., Blumenkranz, M.S., and Constable, I.J. (2019). Three-year follow-up of phase 1 and 2a rAAV.sFLT-1 subretinal gene therapy trials for exudative age-related macular degeneration. Am. J. Ophthalmol. *204*, 113–123. https://doi.org/10.1016/j.ajo.2019.03.006.
6. Cehajic-kapetanovic, J., Xue, K., Camara, C.M.D., Nanda, A., Wood, L.J., Salvetti, A.P., Dominik, M., Febo, D., Aylward, J.W., Barnard, A.R., et al. (2020). Retinal gene therapy in X-linked retinitis pigmentosa caused by mutations in RPGR: results at 6 months in a first in human clinical trial. Nat. Med. *26*, 354–359. Retinal. https://doi.org/10.1038/s41591-020-0763-1.
7. Cukras, C., Wiley, H.E., Jeffrey, B.G., Sen, H.N., Turriff, A., Zeng, Y., Vijayasarathy, C., Marangoni, D., Ziccardi, L., Kjellstrom, S., et al. (2018). Retinal AAV8-RS1 gene therapy for X-linked retinoschisis: initial findings from a phase I/IIa trial by intravitreal delivery. Mol. Ther. *26*, 2282–2294. https://doi.org/10.1016/j.ymthe.2018.05.025.
8. Tornabene, P., and Trapani, I. (2020). Can adeno-associated viral vectors deliver effectively large genes? Hum. Gene Ther. *31*, 47–56. https://doi.org/10.1089/hum.2019.220.
9. Trapani, I., Colella, P., Sommella, A., Iodice, C., Cesi, G., de Simone, S., Marrocco, E., Rossi, S., Giunti, M., Palfi, A., et al. (2014). Effective delivery of large genes to the retina by dual AAV vectors. EMBO Mol. Med. *6*, 194–211. https://doi.org/10.1002/emmm.201302948.
10. Colella, P., Trapani, I., Cesi, G., Sommella, A., Manfredi, A., Puppo, A., Iodice, C., Rossi, S., Simonelli, F., Giunti, M., et al. (2014). Efficient gene delivery to the cone-enriched pig retina by dual AAV vectors. Gene Ther. *21*, 450–456. https://doi.org/10.1038/gt.2014.8.
11. Vernon, M. (1969). Sociological and psychological factors associated with hearing loss. J. Speech Hear. Res. *12*, 541–563. https://doi.org/10.1044/jshr.1203.541.
12. Fortnum, H.M., Summerfield, A.Q., Marshall, D.H., Davis, A.C., and Bamford, J.M. (2001). Prevalence of permanent childhood hearing impairment in the United Kingdom and implications for universal neonatal hearing screening: questionnaire based ascertainment study. Br. Med. J. *323*, 536–540.
13. Gregory-Evans, K., Pennesi, M.E., and Weleber, R.G. (2013). Retinitis pigmentosa and allied disorders. In Retina, S.J. Ryan, ed., pp. 761–835.
14. Millán, J.M., Aller, E., Jaijo, T., Blanco-Kelly, F., Gimenez-Pardo, A., and Ayuso, C. (2011). An update on the Genetics of usher syndrome. J. Ophthalmol. *2011*, 417217–417218. https://doi.org/10.1155/2011/417217.
15. Panda-Jonas, S., Jonas, J.B., Jakobczyk, M., and Schneider, U. (1994). Retinal photoreceptor count, retinal surface area, and optic disc size in normal human eyes. Ophthalmology *101*, 519–523. https://doi.org/10.1016/S0161-6420(94)31305-4.
16. Remtulla, S., and Hallett, P.E. (1985). A schematic eye for the mouse, and comparisons with the rat. Vis. Res. *25*, 21–31. https://doi.org/10.1016/0042-6989(85)90076-8.
17. Liu, X., Ondek, B., and Williams, D.S. (1998). Mutant myosin VIIa causes defective melanosome distribution in the RPE of shaker-1 mice. Nat. Genet. *19*, 117–118. https://doi.org/10.1038/470.
18. Kolb H. Webvision: The Organization of the Retina and Visual System. University of Utah Health Sciences Center; 1995.
19. Kaufman, P.L., Calkins, B.T., and Erickson, K.A. (1981). Ocular biometry of the cynomolgus monkey. Curr. Eye Res. *1*, 307–309.
20. Jacobson, S.G., Acland, G.M., Aguirre, G.D., Aleman, T.S., Schwartz, S.B., Cideciyan, A.V., Zeiss, C.J., Komaromy, A.M., Kaushal, S., Roman, A.J., et al. (2006). Safety of recombinant adeno-associated virus type 2-RPE65 vector delivered by ocular subretinal injection. Mol. Ther. *13*, 1074–1084. https://doi.org/10.1016/j.ymthe.2006.03.005.
21. Jacobson, S.G., Boye, S.L., Aleman, T.S., Conlon, T.J., Zeiss, C.J., Roman, A.J., Cideciyan, A.V., Schwartz, S.B., Komaromy, A.M., Doobrajh, M., et al. (2006). Safety in nonhuman primates of ocular AAV2-RPE65, a candidate treatment for blindness in Leber congenital amaurosis. Hum. Gene Ther. *17*, 845–858. https://doi.org/10.1089/hum.2006.17.845.
22. Seitz, I.P., Michalakis, S., Wilhelm, B., Reichel, F.F., Ochakovski, G.A., Zrenner, E., Ueffing, M., Biel, M., Wissinger, B., Bartz-Schmidt, K.U., et al. (2017). Superior retinal gene transfer and biodistribution profile of subretinal versus intravitreal delivery of AAV8 in nonhuman primates. Invest. Ophthalmol. Vis. Sci. *58*, 5792–5801. https://doi.org/10.1167/iovs.17-22473.
23. Ye, G.J., Budzynski, E., Sonnentag, P., Nork, T.M., Miller, P.E., Sharma, A.K., Ver Hoeve, J.N., Smith, L.M., Arndt, T., Calcedo, R., et al. (2016). Safety and biodistribution evaluation in cynomolgus macaques of rAAV2tYF-PR1.7-hCNGB3, a

recombinant AAV vector for treatment of achromatopsia. Hum. Gene Ther. Clin. Dev. *27*, 37–48. https://doi.org/10.1089/humc.2015.164.

24. Vandenberghe, L.H., Bell, P., Maguire, A.M., Cearley, C.N., Xiao, R., Calcedo, R., Wang, L., Castle, M.J., Maguire, A.C., Grant, R., et al. (2011). Dosage thresholds for AAV2 and AAV8 photoreceptor gene therapy in monkey. Sci. Transl. Med. *3*, 88ra54. https://doi.org/10.1126/scitranslmed.3002103.

25. Ail, D., Ren, D., Brazhnikova, E., Nouvel-Jaillard, C., Bertin, S., Mirashrafi, S.B., Fisson, S., and Dalkara, D. (2022). Systemic and local immune responses to intraocular AAV vector administration in non-human primates. Mol. Ther. Methods Clin. Dev. *24*, 306–316. https://doi.org/10.1016/j.omtm.2022.01.011.

26. Sahly, I., Dufour, E., Schietroma, C., Michel, V., Bahloul, A., Perfettini, I., Pepermans, E., Estivalet, A., Carette, D., Aghaie, A., et al. (2012). Localization of usher 1 proteins to the photoreceptor calyceal processes, which are absent from mice. J. Cell Biol. *199*, 381–399. https://doi.org/10.1083/jcb.201202012.

27. Reichel, F.F., Dauletbekov, D.L., Klein, R., Peters, T., Ochakovski, G.A., Seitz, I.P., Wilhelm, B., Ueffing, M., Biel, M., Wissinger, B., et al. (2017). AAV8 can induce innate and adaptive immune response in the primate eye. Mol. Ther. *25*, 2648–2660. https://doi.org/10.1016/j.ymthe.2017.08.018.

28. Tao, L.W., Wu, Z., Guymer, R.H., and Luu, C.D. (2016). Ellipsoid zone on optical coherence tomography: a review. Clin. Exp. Ophthalmol. *44*, 422–430. https://doi.org/10.1111/ceo.12685.

29. Rodríguez-Bocanegra, E., Wozar, F., Seitz, I.P., Reichel, F.F.L., Ochakovski, A., Bucher, K., Wilhelm, B., Bartz-Schmidt, K.U., Peters, T., and Fischer, M.D.; RD-CURE Consortium (2021). Longitudinal evaluation of hyper-reflective foci in the retina following subretinal delivery of adeno-associated virus in non-human primates. Transl. Vis. Sci. Technol. *10*, 15. https://doi.org/10.1167/tvst.10.6.15.

30. Dimopoulos, I.S., Hoang, S.C., Radziwon, A., Binczyk, N.M., Seabra, M.C., MacLaren, R.E., Somani, R., Tennant, M.T.S., and MacDonald, I.M. (2018). Two-year results after AAV2-mediated gene therapy for choroideremia: the alberta experience. Am. J. Ophthalmol. *193*, 130–142. https://doi.org/10.1016/j.ajo.2018.06.011.

31. Liu, X., Vansant, G., Udovichenko, I.P., Wolfrum, U., and Williams, D.S. (1997). Myosin VIIa, the product of the Usher 1B syndrome gene, is concentrated in the connecting cilia of photoreceptor cells. Cell Motil Cytoskeleton *37*, 240–252. https://doi.org/10.1002/(SICI)1097-0169(1997)37:3<240::AID-CM6>3.0.CO;2-A.

32. Liu, X., Udovichenko, I.P., Brown, S.D., Steel, K.P., and Williams, D.S. (1999). Myosin VIIa participates in opsin transport through the photoreceptor cilium. J. Neurosci. *19*, 6267–6274. https://doi.org/10.1523/jneurosci.19-15-06267.1999.

33. Nathwani, A.C., Gray, J.T., Ng, C.Y.C., Zhou, J., Spence, Y., Waddington, S.N., Tuddenham, E.G.D., Kemball-Cook, G., McIntosh, J., Boon-Spijker, M., et al. (2006). Self-complementary adeno-associated virus vectors containing a novel liver-specific human factor IX expression cassette enable highly efficient transduction of murine and nonhuman primate liver. Blood *107*, 2653–2661. https://doi.org/10.1182/blood-2005-10-4035.

34. Grimm, D., Kern, A., Rittner, K., and Kleinschmidt, J.A. (1998). Novel tool for production and purification recombinant adenoassociated virus vectors. Hum. Gene Ther. *9*, 2745–2760.

35. Liu, Y.L., Wagner, K., Robinson, N., Sabatino, D., Margaritis, P., Xiao, W., and Herzog, R.W. (2003). Optimized production of high-titer recombinant adeno-associated virus in roller bottles. Biotechniques *34*, 184–189. https://doi.org/10.2144/03341dd07.

36. Salvetti, A., Orève, S., Chadeuf, G., Favre, D., Cherel, Y., Champion-Arnaud, P., David-Ameline, J., and Moullier, P. (1998). Factors influencing recombinant adeno-associated virus production. Hum. Gene Ther. *9*, 695–706. https://doi.org/10.1089/hum.1998.9.5-695.

37. Zolotukhin, S., Byrne, B.J., Mason, E., Zolotukhin, I., Potter, M., Chesnut, K., Summerford, C., Samulski, R.J., and Muzyczka, N. (1999). Recombinant adeno-associated virus purification using novel methods improves infectious titer and yield. Gene Ther. *6*, 973–985. https://doi.org/10.1038/sj.gt.3300938.

38. Doria, M., Ferrara, A., and Auricchio, A. (2013). AAV2/8 vectors purified from culture medium with a simple and rapid protocol transduce murine liver, muscle, and retina efficiently. Hum. Gene Ther. Methods *24*, 392–398. https://doi.org/10.1089/hgtb.2013.155.

39. Liang, F.-Q., Anand, V., Maguire, A.M., and Bennett, J. (2001). Intraocular delivery of recombinant virus. Methods Mol. Med. *47*, 125–139. https://doi.org/10.1385/1-59259-085-3:125.